Interfacial Tension of a Liquid Crystalline Polymer in an Isotropic Polymer Matrix

Jian Wu and Patrick T. Mather*,†

Chemical Engineering Department and Polymer Graduate Program, Institute of Materials Science, University of Connecticut, Storrs, Connecticut 06269-3136

Received March 7, 2005; Revised Manuscript Received June 18, 2005

ABSTRACT: We investigated the interfacial tension of a thermotropic liquid crystalline polymer (LCP) embedded in a flexible isotropic matrix, poly(dimethylsiloxane) (PDMS), using a modified deformed droplet retraction method (MDDR). The thermotropic polymer employed, PSHQ-6,12, was nematic and featured a well-defined nematic−isotropic clearing transition temperature so that MDDR experiments could be conducted over a temperature range spanning nematic, isotropic, or biphasic regions for the droplet phase. Our results showed that the interfacial tension for temperatures in the nematic range of the droplet is ∼5 mN/m and increases slightly with temperature. Within the isotropic phase, the interfacial tension is significantly higher, starting at a value greater than 20 mN/m and decreasing with temperature with a slope of −0.3 mN/(m K). On crossing the transition from a nematic to isotropic phase for the LCP, the interfacial tension increases in a nearly stepwise manner. Imaging of both retardance and orientation with compensated polarizing optical microscopy clearly revealed homeotropic orientation of the LCP near the LC/isotropic interface, especially below the bulk isotropization temperature, but also for temperatures near, but above, this temperature. We conclude that the interfacial tension for this system is sensitive to the level of nematic ordering at the interface, with homeotropic anchoring yielding significantly lower values than an interface with no preferential anchoring.

Introduction

Blending immiscible polymers is a widely employed method to create new materials with properties bridging those of the two components, sometimes with synergism. As a particular approach, the addition of a minor amount of liquid crystalline polymer (LCP) to an isotropic polymer may yield high strength materials[1] with the additional advantage of viscosity reduction. In some processing flows, the LCP-rich phase can form fibrillar inclusions resulting in a "self-reinforced" blend,[2,3] the properties of which strongly depend on phase distribution (morphology) that, in turn, depends on component rheology, interfacial tension, volume fraction, and flow kinematics. As with conventional immiscible blends, the interfacial tension in LCP blends influences droplet breakup and coalescence and governs the deformation of droplets to fibrils.[4] Although many scientists have measured the surface tension[5−8] and interfacial tension[9,10] of small molecule liquid crystals, very limited attention has been given to interfacial tension of polymeric liquid crystals,[11−13] and systematic studies on its temperature dependence are absent.

A variety of experimental methods have been developed for determining the interfacial tension between polymeric fluids, and the subject has recently been reviewed.[14] The methods can be divided into three categories: (1) equilibrium, (2) rheological, and (3) microscopic dynamic methods. The equilibrium methods include the "pendant drop", "sessile drop", and "spinning drop" techniques. For each of these, accurate data for the density difference between the two liquid polymers, usually very small, are required and appear in leading order with respect to the interfacial tension measurement. In addition, because polymeric fluid viscosities are generally high, equilibration times may be so long as to risk thermal degradation. Rheological methods, on the other hand, are based on linear viscoelastic measurements of blend samples for which interfacial tension contributes to modification of the low-frequency storage modulus. With independent knowledge of the average droplet diameter, fitting of the viscoelastic spectrum with theoretical models (Palierne[15] or Bousmina[16] model) allows estimation of the interfacial tension. To date, a number of researchers have successfully employed this method to determine the interfacial tension.[14,17−19]

Microscopic dynamic methods mainly include the breaking thread[20] and deformed droplet retraction[21] experiments, among others. In these methods, the interfacial tension is determined by observing shape evolution with time of one phase embedded in another, driven by interfacial tension and resisted by viscous dissipation. Comparison with a model can allow extraction of interfacial tension to the extent that the matrix and droplet viscosities are known. Although both the breaking thread and deformed droplet retraction methods are attractive in their simplicity and applicability to polymeric liquids, they also have disadvantages. For the breaking thread method, it is experimentally difficult to start with a perfectly uniform radius and symmetric initial perturbation. Further, residual stress from filament processing may lead to artificially high interfacial tension measurements. In the deformed droplet retraction method, the major axis of a droplet deformed by application of a shear pulse generally has a nonzero angle with the observation plane, making measurements of its length difficult. Moreover, normal stresses in the matrix fluid may flatten the droplet during shear deformation, complicating subsequent quiescent shape evolution. We note that Lee and Denn[22]

† Present address: Macromolecular Science and Engineering, Case Western Reserve University, Cleveland, OH 44106.
* Corresponding author. E-mail patrick.mather@case.edu.

10.1021/ma050483x CCC: $30.25
Published on Web 07/21/2005

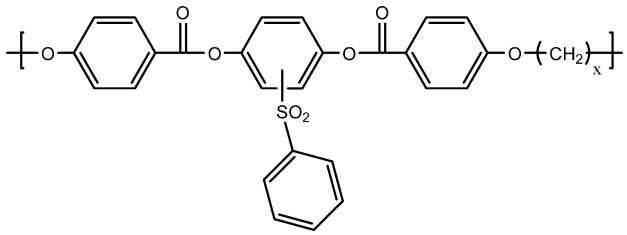

Figure 1. Chemical structure of poly[(phenylsulfonyl)-*p*-phenylene alkylene-bis(4-oxybenzoate)]. PSHQ-6,12 is a 50:50 mol % copolymer with $x = 6, 12$.

studied the retraction of deformed thermotropic LCP droplets in an isotropic polymer matrix; however, extraction of interfacial tension from the observations was not pursued, presumably due to very large droplet deformations that we discuss later.

To overcome these disadvantages, the breaking thread and deformed droplet retraction methods can be combined.[23,24] In particular, the combined method involves examination of ellipsoidal drops formed after the capillary instability of the breaking thread method has progressed to the point of pinching off of droplets. The ellipsoidal droplets then retract to equilibrium spheres. By measuring the shape evolution of a selected droplet, one can determine the interfacial tension in the system using Taylor theory.[25] The method addresses well problems of the previously mentioned dynamic methods: (1) the strict requirement for uniform shape and diameter of the fiber is removed, and (2) the deformed drop is naturally axisymmetric with the long axis orientation controlled by original fiber placement in the matrix. Experimental results[23,24] show that the measured interfacial tension values are quite close to those data determined by other methods, even for matrix viscosity and inclusion/matrix viscosity ratio covering a rather wider range. We refer to this method throughout as the modified deformed droplet retraction (MDDR) method.

In this paper, we determined the interfacial tension between a thermotropic liquid crystalline polymer droplet and an isotropic polymer matrix over a range of temperatures by employing the MDDR method. To further understand our findings, information pertaining to the molecular orientation at the nematic−isotropic interface is obtained using quantitative birefringence and orientation angle imaging.

Experimental Section

Materials. The materials used here include (1) the isotropic polymer matrix poly(dimethylsiloxane) (PDMS from Rheometric Scientific, Inc.) and (2) the liquid crystalline polymer poly[(phenylsulfonyl)-*p*-phenylene alkylene-bis(4-oxybenzoate)] having 50 mol % of a 6-methylene spacer and 50 mol % of a 12-methylene spacer (PSHQ-6,12 from Prof. C. D. Han's group[26]). Its chemical structure is shown in Figure 1. The mesogenic unit is incorporated along the polymer main chain in a segmented fashion. The PDMS selected is a viscoelastic liquid with a viscosity of $\sim 1.0 \times 10^4$ Pa·s at 25 °C. By comparison, PSHQ-6,12 is a glassy nematic polymer with a glass transition temperature $T_g = 85$ °C and with crystallization suppressed by a combination of the bulky pendant group and copolymerization. Above T_g, PSHQ-6,12 softens to a nematic liquid and, with continued heating, undergoes a nematic−isotropic phase transition centered at $T_{NI} = 185.6$ °C. Both T_g and T_{NI} were obtained from the second scan DSC curve measured by a TA Instruments 2920 MDSC with a heating rate of 10 °C/min.

Rheological Measurements. Applying Taylor theory[25] to the analysis of droplet retraction observations requires accurate zero-shear viscosity measurements for the fluids involved, especially the continuous phase but also the droplet phase through its appearance in the viscosity ratio (details appear below). Accordingly, a TA Instruments ARES rotational rheometer was employed to conduct dynamic oscillatory shear measurements spanning a wide range of frequencies and temperatures for both PDMS and PSHQ-6,12. Two shearing geometries were employed: 25 mm parallel plates for PDMS and 8 mm cone−plate (5° cone angle) for PSHQ6,12, the latter being selected primary due to limited sample availability.

The rheological behavior of thermotropic liquid crystalline polymers depends heavily on previous thermal and deformation history through a highly variable orientationally anisotropic state. More specifically, the rheological behavior is the reflection of the internal microstructure, a finding studied in detail in the past.[27,28] To obtain PSHQ-6,12 rheological data relevant to our interfacial tension measurements, we designed a certain experimental protocol: Specimens were first heated to prescribed temperature within the nematic phase and sheared at $\dot{\gamma} = 0.1$ s^{-1} for 200 s.u. (one rotation), heated to 200 °C (isotropic phase), and finally cooled to a predetermined temperature (nematic phase; same as for preshearing) for the measurement of complex viscosity. This thermomechanical protocol was designed to reproduce the orientational history of the LCP thread breakup and subsequent droplet retraction as much as possible.

Specimen Preparation. PSHQ-6,12 fibers were manually drawn from the melt at 200 °C using tweezers withdrawn from a 30−50 mg pool of molten polymer at a speed of ~0.25 m/s. Such prestretched fibers were cut into short sections featuring aspect ratios L/D > 50 and dried in under vacuum for 1 day at $70 < T < 80$ °C, a temperature just below T_g. Meanwhile, the matrix material, PDMS, was dried and degassed in the form of two coverslip coatings (1 mm thick) at 140 °C. To embed the LCP within PDMS, a PSHQ-6,12 fiber section, prepared as detailed above, was placed on the top of one of the coatings and the second PDMS coating/cover slide introduced so as to sandwich the fiber within a surrounding PDMS matrix. Care was taken to avoid entrapment of air at the LCP/PDMS interface that could be easily visualized upon heating within the hot-stage microscope. As prepared, the fibers of such specimens feature residual stress from the fiber drawing preparation, and this stress was relaxed by annealing at a temperature above T_g but low enough to avoid premature Rayleigh breakup, as described below.

Interfacial Tension Measurements. Specimens prepared as above were placed into a microscope hot stage (Instec STC200E) mounted on a transmission polarized optical microscope (POM, Olympus BX-50), with which the observation of the time evolution of PSHQ-6,12 droplet shapes is carried out. The digital images from the POM were captured using a Panasonic CCD camera (model GP-KR222) and frame grabber. Spatial dimensions were calibrated using a stage micrometer with 10 μm line spacing. To relax any axial stress in the fibers, the hot stage was first elevated to 120 °C and maintained there for 10 min, during which time slight axial contraction was observed. Next, to obtain a reproducible initial state of the nematic phase, the specimens were quickly raised to 200 °C, where the samples cleared to the isotropic phase, and then cooled to a prescribed test temperature. This flash heating was short enough in duration to avoid any fiber distortion as driven by interfacial tension. As time then elapsed at the test temperature, the fibers underwent sinusoidal distortion, as expected, and then disintegrated into drops, the shapes of which were not immediately ellipsoidal due to sharp tips that remain directly following pinch-off. Digital micrographs were not collected for analysis until after several minutes, a delay time following pinch-off that preliminary experiments revealed to be sufficient to yield ellipsoids distorted from only slightly from a spherical shape ($D \sim 10\%$, see below).

Orientation Measurements. To quantitatively map director order and orientation within PSHQ-6,12 droplets, we exploited automated compensation techniques for polarizing optical microscope developed earlier for the imaging of living cells[29,30] and then commercialized by CRI Inc. as LC-Polscope.

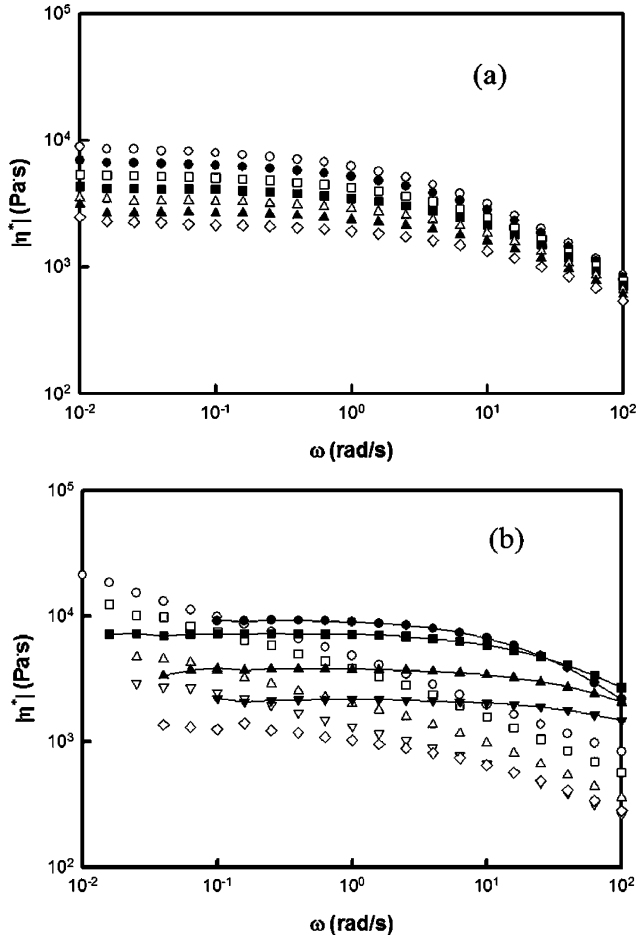

Figure 2. (a) Magnitude of complex shear viscosity, $|\eta^*(\omega)|$, vs frequency for PDMS at different temperatures: (○) 100, (●) 120, (□) 140, (■) 160, (△) 180, (▲) 200, and (◇) 220 °C and (b) PSHQ6,12 at (○) 140, (□) 150, (△) 160, (▽) 170, (◇) 180, (●) 185, (■) 200, (▲) 210, and (▼) 220 °C.

The instrument employs filtered (546 nm) circularly polarized light that transmits through the samples and then passes through a stacked two-component liquid crystal compensator under time-sequenced computer control. A stack of four images acquired under distinct compensator states is then analyzed to quickly yield separate quantitative images of retardance (ΔnL < 273 nm; L = path length) and slow-axis orientation. For materials with positive birefringence, the slow-axis orientation is coincident with the director orientation, while for those with negative birefringence the two are orthogonal. To our knowledge, no reports employing LC-Polscope (or similar) methods to characterize the orientation of liquid crystalline systems have appeared to date. Thus, the retardance and slow-axis orientation in the form of 640 × 480 images for PSHQ-6,12 droplets in a PDMS matrix were measured using the LC-Polscope in conjunction with an Olympus BX-50 microscope.

Results and Discussion

Pure Component Properties. To obtain the zero-shear viscosity values for each component, we conducted dynamic oscillation frequency sweeps for a range of temperatures. Figure 2a shows the magnitude of the complex viscosity vs frequency (termed hereafter "flow curve") for PDMS, revealing a simple response. For low frequencies a clear Newtonian viscosity plateau appears and is followed by shear thinning at high frequencies. In contrast, flow curves for PSHQ-6,12 from 140 to 220 °C are more complex. As shown in Figure 2b, within the isotropic phase (above T_{NI}, filled symbols), the rheology of PSHQ-6,12 is simple like PDMS; however,

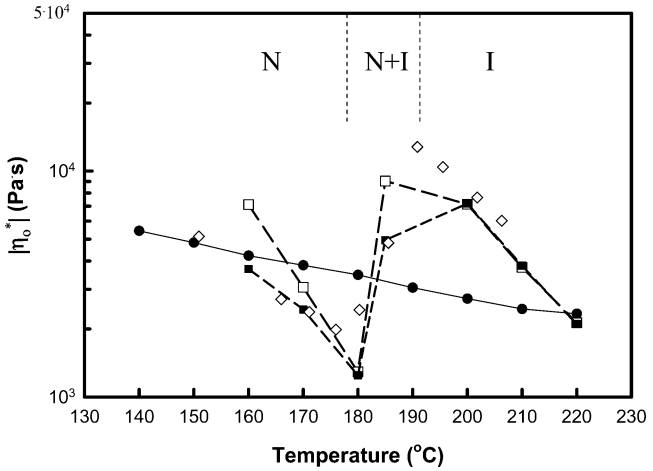

Figure 3. Zero-shear viscosity of PDMS and PSHQ6,12 at different temperatures: (●) PDMS, (□) PSHQ6,12, and (■) PSHQ6,12 (0.1 rad/s). The zero viscosity is estimated by fitting the experiment data shown in Figure 2 with the Carreau-O model. For comparison, steady shearing data[27] for $\dot{\gamma}$ = 0.1 s^{-1}(◇) is also shown. Vertical dashed lines indicate the onset and completion points for PSHQ-6,12 isotropization from DSC (second heat, 10 °C/min).

the behavior is more complicated within the nematic phase (below T_{NI}, open symbols). For temperatures low compared to T_{NI} ($T \leq 150$ °C), a clear Newtonian plateau is not obtained at low frequency, viscosity continuing to rise monotonically. However, there is a nematic temperature range (160 < T < 175 °C) where a Newtonian plateau is observed, for ω < 0.1 rad/s, approximately. Near and crossing the nematic−isotropic transition temperature from below, the rheological behavior of PSHQ-6,12 becomes increasingly similar in shape to that of the isotropic phase, i.e., simple with a Newtonian plateau. Fitting all of the frequency sweep data with the Carreau-O model then allowed extraction of the zero-shear viscosity of PDMS and PSHQ6,12, the results of which are shown in Figure 3. The zero-shear viscosity of PDMS decreases with increasing temperature. Meanwhile, in agreement with a previous report using steady shearing flow,[27] PSHQ-6,12 features a stepwise increase of zero shear viscosity at the nematic−isotropic transition temperature. Within the pure nematic and isotropic phases, the zero-shear viscosity monotonically decreases with temperature with negative slopes that are substantially larger than for PDMS. By comparison of dynamic oscillatory data at a selected frequency (ω = 0.1 rad/s) with the steady shearing data ($\dot{\gamma}$ = 0.1 s^{-1}) of Chang and Han,[27] the expected agreement between steady and oscillatory shear viscosity measurements at low deformation rates was satisfied. This implies the absence of a yield stress for the range of temperatures studied.

Interfacial Tension. Rigorously, the MDDR method used here is only valid for Newtonian droplets in a Newtonian matrix. To extend this method to viscoelastic materials, the following two conditions should be satisfied: (1) the droplet deformations are small enough (D < 15%) so that the dynamics are independent of initial deformation, and (2) any molecularly based elastic relaxation following deformation occurs much faster than the rate of ellipsoidal droplet retraction. Inspecting the flow curves of the two materials, we find that the longest relaxation time of PDMS sample is ca. 0.1−1.0 s, while for PSHQ-6,12 the longest relaxation time is around 0.02 s or even shorter in the isotropic

phase, depending on temperature. Within the nematic phase, if the temperature is close to nematic−isotropic transition (160 < T < 180 °C), the longest relaxation time (whether molecular or texture-based) is significantly slower: 10 to 60 s. At still lower temperatures (T < 150 °C), this time cannot be estimated from the dynamic frequency sweep spectrum. In other words, the elastic relaxation time is rather long. Thus, the temperatures chosen in our experiments were restricted to the range 160 < T < 220 °C, and droplet sizes were selected, through iteration, to yield characteristic retraction times greater (at least double) than the LCP relaxation time. In practice, following fiber pinch-off we wait several minutes for the droplets to become ellipsoidal before measuring the droplet deformation evolution, $D(t)$. Considering all of these factors, we are confident that the droplet relaxation dynamics we report involve only the interfacial tension driving force and Newtonian fluid mechanics accounted for by Taylor.[25] In this scenario, the shape evolution of deformed ellipsoidal drops should follow

$$D = D_0 \exp\left[-\frac{40(p+1)}{(2p+3)(19p+16)}\frac{\sigma}{\eta_m R_0}t\right] \quad (1)$$

Here, D is the droplet deformation defined as $D = (L - B)/(L + B)$, and L and B are the lengths of the ellipsoidal droplet's major and minor axes, respectively. D_0 is an initial droplet deformation, σ is the interfacial tension, η_m is the matrix viscosity, R_0 is the equilibrium radius, p is the viscosity ratio of the dispersed phase (η_d) over the matrix phase (η_m), and t is time. Plotting $\ln(D/D_0)$ vs t then allows interfacial tension (σ) estimation from the plot's slope.

In light of eq 1, an interfacial relaxation time (τ_σ) for deformed droplet retraction can be defined as

$$\tau_\sigma = \frac{\eta_{eq} R_0}{\sigma} \quad (2)$$

where η_{eq} is defined as equivalent viscosity

$$\eta_{eq} = \frac{(2p+3)(19p+16)}{40(p+1)}\eta_m \quad (3)$$

η_m being the zero-shear viscosity of matrix (PDMS). Since equivalent viscosity and interfacial tension each derive from material properties, the droplet size is the only adjustable variable from experiment to experiment, τ_σ increasing in proportion to droplet size. Thus, increasing the drop size is another effective way to ensure that interfacial relaxation is slow enough not to overlap with molecular relaxation times of the droplet or matrix. In our experiment, the droplet size chosen is around 100 μm or larger; i.e., the original filament diameters were chosen so that πD > 100 μm. For example, a 100 μm of PSHQ-6,12 droplet in PDMS at 220 °C would feature $\tau_\sigma \approx 30$ s for $\sigma = 15$ mN/m.

Since PSHQ-6,12 is a thermotropic liquid crystalline polymer, effects of a liquid crystalline origin (microstructural or dynamic) have to be considered. On the basis of prior reports for this polymer,[26,27] the texture scale is in the range 1−10 μm, noting that this length depends on coarsening time and deformation history. If the droplet size is comparable with this liquid crystalline texture length, droplet retraction will follow surface-modified nematodynamics[31] with a monodomain characteristic relaxation time $\tau_n = (\eta/K)d_n^2$, where η is the nematic viscosity, K is an elastic constant, and d_n is the texture domain size. However, the thermal treatment of first clearing the LCP fibers (described above) yields a highly disordered internal texture for which $d_n \ll d_f$, where d_f is the fiber diameter. As shown in Figure 4, the extended PSHQ6,12 fiber breaks up into a sequence of ellipsoidal droplets, each (last picture in Figure 4) being very dark due to small d_n. In contrast, the thinning portions of the precursor LCP fiber experiencing extensional flow become quite birefringent and nearly free of defects—such satellite droplets, while interesting, are not considered for interfacial tension measurements. Because $d_n \ll d_f$ for cases considered here, we are confident that nematodynamics, beyond determining η_{LCP}, do not play an important role in determining the rate of droplet retraction.

After the LCP fiber disintegrates, the formed ellipsoid-like drops retract to equilibrium spherical droplets. Figure 5 shows the typical retraction of an example nematic PSHQ-6,12 (T = 160 °C) ellipsoidal droplet in PDMS, viewed without the analyzer, where a characteristic time scale of order 100 s is observed. We observe a lack of any textural coarsening, as would be manifested in higher light transmission, for the droplet in Figure 5 and all other similar experiments. In contrast, textural coarsening was clearly observed in the thinning (extensional flow) regions of the thread breakup experiments (Figure 4), and these dynamics warrant further study. The two tips of the major axis of the deformed drop are maintained in clear focus during image acquisition, ensuring us that the major axis remains parallel to the observation plane as we anticipated. In Figure 6, we report example experimental contours of a PSHQ-6,12 droplet at initial (0 s) and late (1060 s) stages, each well fit by an ellipsoidal shape. The volume of the observed droplet can then be calculated for ellipsoids to be $V = (\pi/6)LB^2$, where L and B are major and minor axis lengths. We observed for all cases (Supporting Information) that V is time-invariant and equal to the equilibrium volume, $V = (4/3)\pi R_0^3$. This finding provides further evidence that the major axis remains parallel to the observation plane and that the droplet cross section is circular. Meanwhile, the initial deformations (D_0) are ca. 10.5%, small enough to safely apply the MDDR method. Recently, Lee and Denn[22] found that the initial deformation (strain) has a strong influence on the retraction behavior of LCP (Vectra B950) droplets. However, in that study initial deformations were much larger at 100−1000%. Such large deformations could induce textural coarsening within the LCP droplets, which would explain the observed deformation dependence.

By inspection of eqs 1−3, plots of $\ln(D/D_0)$ vs $t/(\eta_{eq}R_0)$ will clearly show variation in interfacial tension (σ) through slope differences. Figure 7 shows such plots for temperatures spanning 160 < T < 220 °C. Within the biphase and isotropic phase, there is only one characteristic negative slope for the entire time span observed, as shown in Figure 7a. However, within the nematic phase, the plots feature a transition from a steep (though linear) slope to a shallow one, i.e., from higher to lower σ. To proceed, we estimated the interfacial tension for these cases in two regimes: one for the early retraction stage ($t/(\eta_{eq}R_0)$ < 300), shown in Figure 7b, and the other from the late stage shown in Figure 7a.

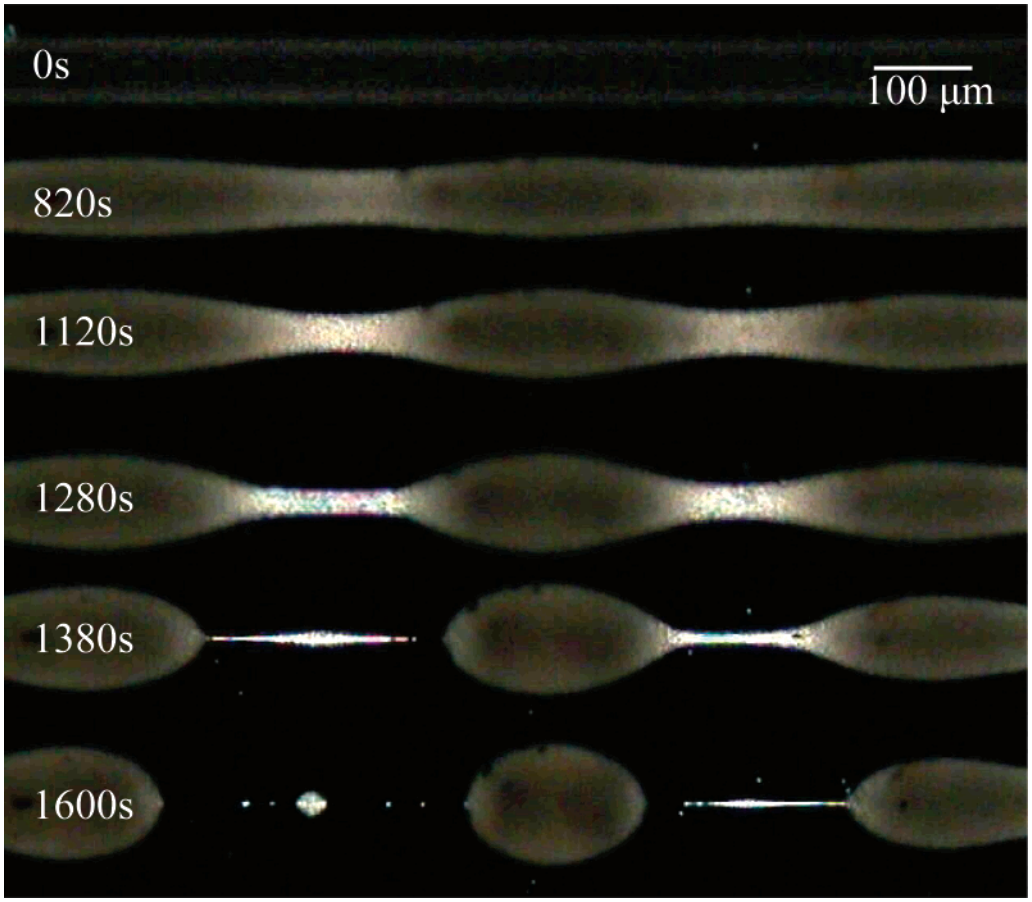

Figure 4. Observation of sinusoidal distortion on a predisoriented PSHQ-6,12 fine fiber embedded in PDMS matrix at 160 °C by polarized optical microscope (POM). The fiber is 45° with respect to the crossed polarizer and analyzer.

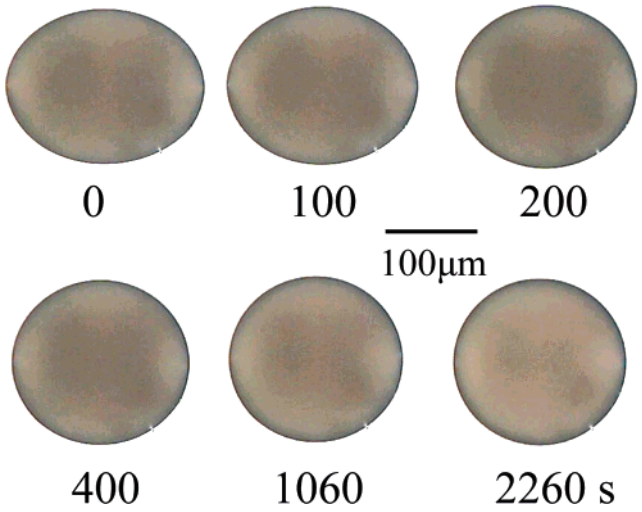

Figure 5. Time evolution of an ellipsoidal PSHQ-6,12 drop in the PDMS matrix at 160 °C prepared from the disintegration of prestretched PSHQ-6,12 fibers at 160 °C. Micrograph acquisition commenced only after several minutes, when the droplet shapes have become ellipsoidal.

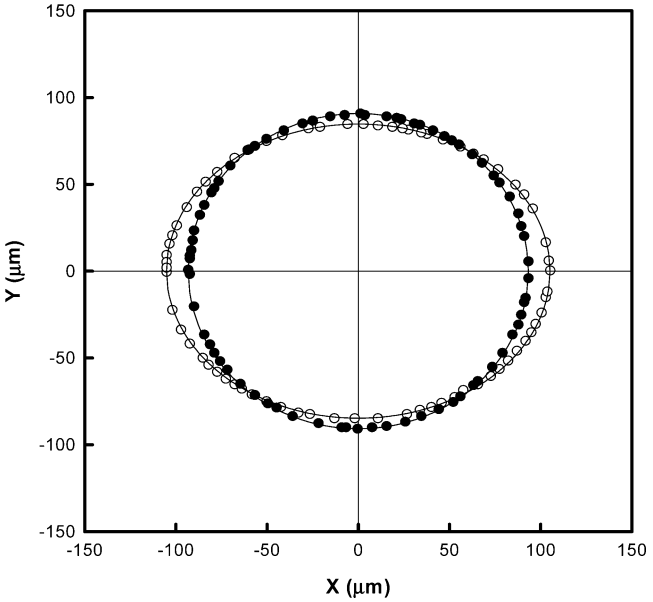

Figure 6. Comparison of PSHQ-6,12 droplet surface contour (symbols) and equivalent ellipse (lines). Experimental contour correspond to the droplet shown in Figure 5 at different time: (○) 0 and (●) 1060 s. The X- and Y-axes represent the major and minor axis of PSHQ-6,12 ellipsoidal droplet, respectively. The typical initial deformation, $D_0 = (L_0 - B_0)/(L_0 + B_0)$, is equal to 10.5% (or $(L_0 - 2R_0)/2R_0 = 15.0\%$).

The estimated interfacial tension for the PSHQ-6,12/PDMS interface is plotted as a function of temperature in Figure 8. Within the nematic phase, whether estimated from the early or late stages, interfacial tension increases slowly with temperature. However, interfacial tension values estimated at the early stage are approximately 10-fold larger than those estimated from the late stage. In addition, the temperature dependence of interfacial tension ($d\sigma/dT$) is small and positive: ca. 0.075 and 0.12 mN/(m K) for the early and late stages, respectively. Within the biphasic regime, interfacial tension features a stepwise increase, much like the temperature dependence of viscosity for the LCP (Figure

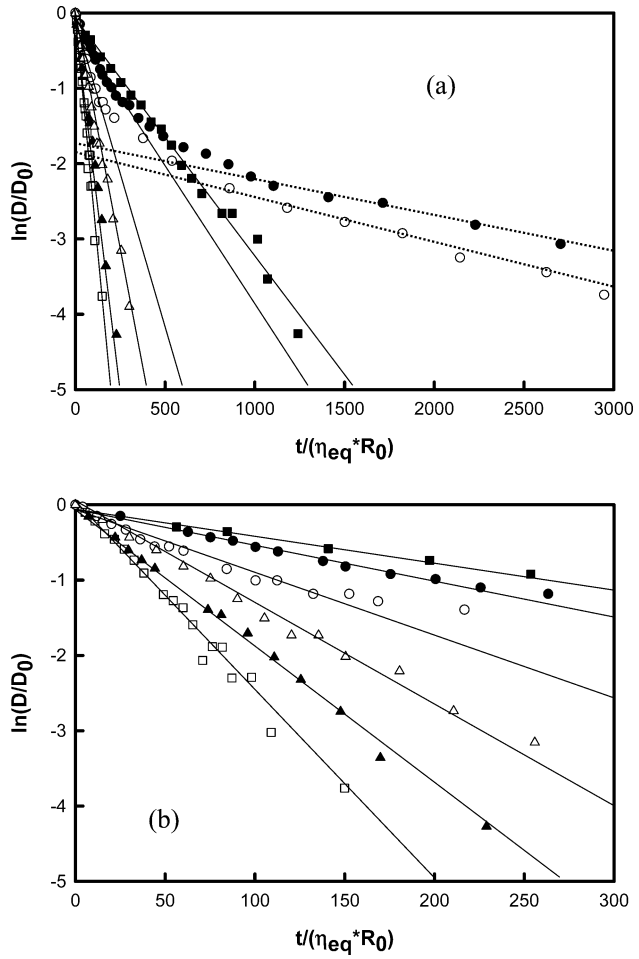

Figure 7. Plot of $\ln(D/D_0)$ vs $t/(\eta_{eq}R_0)$ for the ellipsoidal PSHQ-6,12 drop in the PDMS matrix, describing (a) droplet deformation vs time and (b) early stage behavior at different temperatures: (●) 160, (○) 170, (■) 180, (□) 190, (▲)200, and (△) 220 °C.

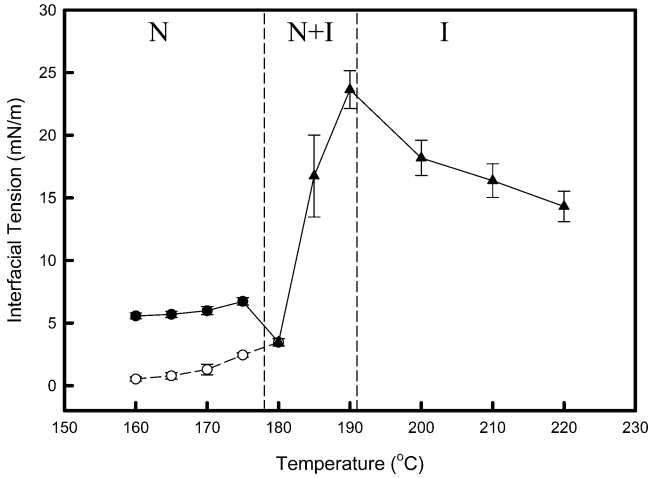

Figure 8. Interfacial tension between PSHQ-6,12 and PDMS at different temperatures: (▲) at biphase and isotropic phase; at nematic phase, (●) and (○) represent the interfacial tension estimated from early and late stage of deformed PSHQ-6,12 droplet retraction, respectively. Vertical dashed lines indicate the onset and completion points for PSHQ-6,12 isotropization from DSC (second heat, 10 °C/min).

3) but having adequately accounted for the viscosity step via eqs 1−3 and earlier reported viscosity measurements. The interfacial tension reaches a maximum value at the point of complete isotropization and then decreases within the isotropic phase with a rather large negative slope ($d\sigma/dT \cong -0.30$ mN/(m K)).

The results shown in Figure 8 are initially surprising, though strikingly similar in temperature dependence to the interfacial tension of 5CB (*n*-pentylcyanobiphenyl, a low molar mass nematic) in water, measured using tensiometry[10] at least for particular 5CB density data. Additionally, the temperature dependence of LC−air surface tension shows similar anomalous behavior[5] (though with larger values, quantitatively, as expected). In light of Rai and Denn's data[9] that showed minimal step-up in γ for 5CB in PDMS, Kim et al.[10] have pointed out that the exact interfacial tension measurements depend strongly on density measurements for 5CB and 8CB that are, unfortunately, an issue of some debate. However, the trend in interfacial tension vs temperature is preserved to be increasing, as simulations also indicated.[32]

Bulk Director Distribution. While we were unable to directly observe LCP director distribution optically due to very fine textures, we did observe a profound manifestation of it: anisotropic thermal contraction of the droplets during cooling after retraction. Such shape evolutions for PSHQ-6,12 droplets during the cooling are shown in Figure 9 for cases where the droplets had fully retracted in either (a) the nematic state or (b) the isotropic state. For the nematic case, the resulting droplet exhibits anisotropy wherein its initial major axis contracts more extensively than its initial minor axis, resulting in an oblate ellipsoid whose long axis is oriented orthogonal to the original fiber axis. Given that experiments on other thermotropic LCPs have shown an anisotropic coefficient of thermal expansion (CTE) with significantly larger CTE transverse to the primary orientation direction,[33] this observation seems consistent with a postulated orientation distribution drawn in Figure 9, superimposed with an average orientation direction in the mesoscopic domain sense.[34] For comparison, a PSHQ-6,12 droplet prepared within the isotropic phase (200 °C, Figure 9b) features isotropic shrinkage during cooling, even on passing into the nematic phase, yielding a spherical shape at room temperature. The apparent anisotropy in domain orientation for those ellipsoids retracting in the nematic phase surely originates from flow-orientation coupling, but whether the pertinent flow is that of the early capillary instability or the late droplet retraction is unclear. Experimentally, particle imaging velocimetry (PIV) would be very helpful to provide clarity. Additionally, theoretical modeling of the internal dynamics of textured LCP droplets with various boundary conditions (see below) will be quite helpful in understanding these observations.

Interfacial Director Orientation. As mentioned previously, the nematic orientation at the interface bears great influence on the resulting interfacial tension. On the nematic side of a nematic−isotropic interface, the nematic director may adopt one of several configurations: planar, homeotropic, or oblique. While planar and homeotropic orientations refer to director orientations along or normal to the interface, respectively, an oblique orientation represents an intermediate case. The quantitative consequence of such different orientational states on the interfacial tension is a matter of some debate,[32,35−38] stimulating us to directly examine nematic orientation at the interface experimentally.

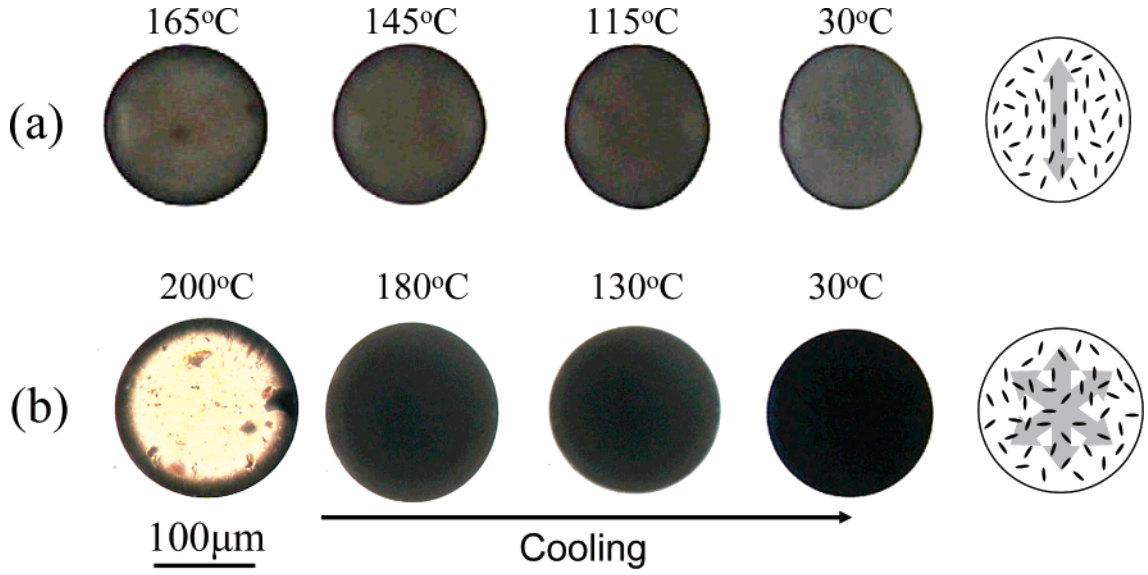

Figure 9. Shape evolution of spherical PSHQ-6,12 droplets, prepared at different temperatures, during the cooling from varying equilibration temperature to room temperature with −10 °C/min ramping rate: (a) 165 vs (b) 200 °C. Schematic diagrams of postulated domain orientation distributions are also shown, superimposed with average orientation.

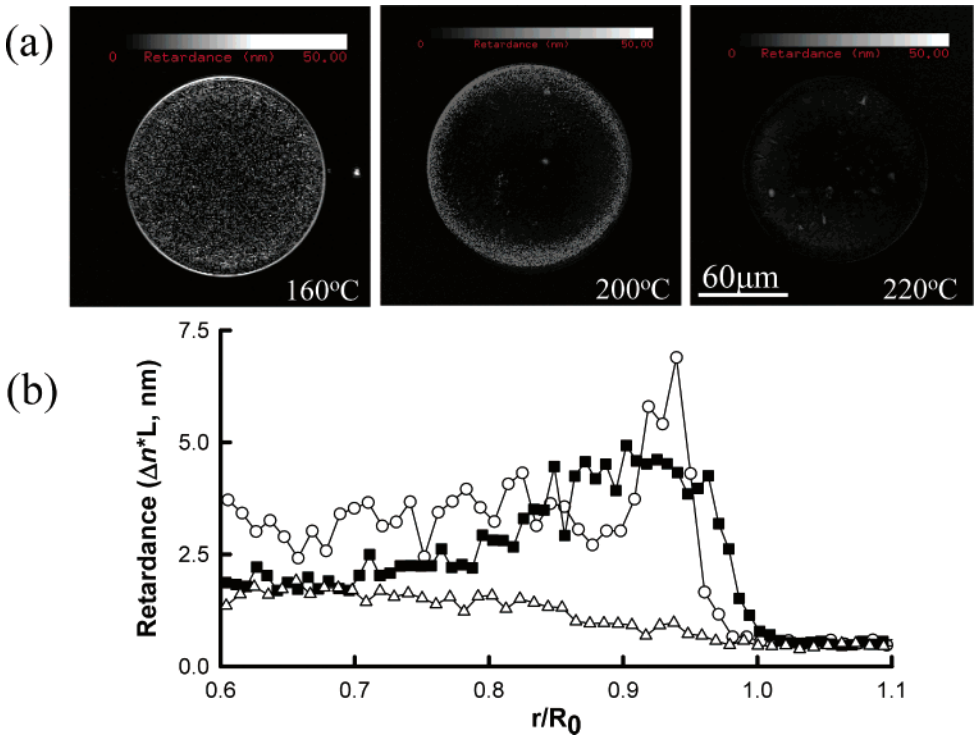

Figure 10. Observations of retardance distribution at the surface of PSHQ-6,12 drop in the PDMS matrix at different temperatures and the corresponding radius distributions of retardance within the droplet: (○) 160, (■) 200, and (△) 220 °C. The gray scale bar represents retardances from 0 to 50 nm for the range of intensities from black to white with 8-bit resolution.

As mentioned in the Experimental Section, we have employed POM with automated compensation techniques to yield quantitative images of optical retardance and slow-axis orientation. While for positive birefringence materials the slow-axis orientation is oriented parallel to the director orientation, the opposite is true for negative birefringence materials. Thus, it was essential for us to determine the sign of birefringence for our PSHQ-6,12 LCP. To do this, we prepared oriented fibers and determined the orientation direction using WAXD analysis and slow-axis orientation with LC-Polscope imaging (Supporting Information), care being taken to use diameters small enough so that the retardance (ΔnL) was less than the upper limit of 273 nm. We found that the orientation direction was axial, while the slow-axis orientation was clearly radial. Thus, PSHQ-6,12 is a negatively birefringent material.

Figure 10a shows the retardance images of spherical PSHQ-6,12 droplets in PDMS matrix after retracting to this shape at different temperatures. At 160 °C (nematic phase), there is a relatively uniform bright ring with higher retardance surrounding the droplet interface. Inside the droplet ($r/R_0 < 0.8$), the retardance and its distribution are not reliable due to scattering from defects. At 200 °C (isotropic phase), the retardance inside the droplet is undetectably low (<2 nm) while, importantly, the interfacial region shows detectable retardance. This clearly indicates persistence of the

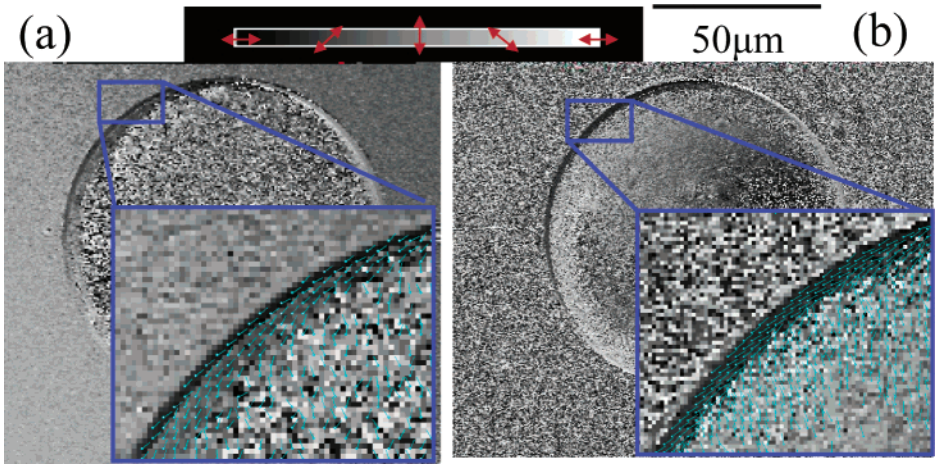

Figure 11. Observations of retardance and slow-axis orientation distribution at the surface of PSHQ-6,12 drop in the PDMS matrix at (a) 160 and (b) 200 °C with 4 nm retardance threshold.

nematic phase at the interface above T_{NI}. When the temperature is raised further to 220 °C, all evidence of liquid crystalline order is erased. Simplistically, three types of LCP droplets within an isotropic matrix are observed: nematic bulk LCP + nematic interfacial LCP (160 °C), isotropic bulk LCP + nematic interfacial LCP (200 °C), and isotropic bulk LCP + isotropic bulk LCP (220 °C).

In better visualize the retardance distribution at the interface and inside the droplet, we measured the radial dependence of retardance ($D = \Delta nL$) as

$$D(r/R_0) = \frac{1}{\pi r}\int_0^{\pi} D(r/R_0,\phi) r \, \mathrm{d}\phi \qquad (5)$$

where r is the distance from center point of the spherical droplet, R_0 is the radius of droplet, and ϕ is azimuthal angle. We note that for our optical arrangement the path length L is approximately the depth of focus of the lens used[30] (~2 μm) and not dependent on the local LCP thickness. Measured in this way, the normalized radial distributions of retardance for the three different temperatures are shown in Figure 10b. At 160 °C, we observe a very sharp peak in retardance at the interface, this peak broadening but not disappearing at 200 °C. In contrast, there is no interfacial retardance peak for T = 220 °C, indicating no interfacial preservation of nematic ordering at this temperature.

It is clear from these observations that the interface features a much higher nematic−isotropic transition (T_{NI}) than the bulk. For instance, at 200 °C ($\approx T_{NI}$ + 10 °C) the interfacial region between the two isotropic phases features nematic order. This intriguing phenomenon is a type of capillary condensation, where a phase transition from a less ordered phase to a more ordered phase is caused by a confined environment. Sheng[39,40] predicted and observed similar capillary condensation for small-molecule nematic liquid crystals. In our case, the nematic anchoring energy[36] between PSHQ-6,12 and PDMS yields a confining environment that raises the local nematic−isotropic transition. To better understand this anchoring, we examined the slow-axis orientation, also with LC-Polscope imaging, noting again that this direction is perpendicular to the nematic director orientation due to the negative birefringence of PSHQ-6,-12.

Figure 11a shows the slow-axis orientation distribution for PSHQ6,12 droplet at 160 °C (bulk nematic phase) following retraction to an equilibrium spherical droplet. Outside of the droplet, in the PDMS liquid, the slow-axis data are incoherent due to the lack of any orientation. At the interface, the slow-axis orientation is oriented parallel to the interface for the outer 12 μm, indicating that the director of this negative-birefringence LCP director anchored homeotropically. At 200 °C (bulk isotropic phase), the interface can be seen as a thin layer (7 μm thick), still homeotropic, confined between the two large isotropic phases (Figure 11b). Comparing Figure 11b with Figure 10 for the same temperature, we find that only a fraction (roughly 50%) of the surface-induced nematic order is well-oriented.

Discussion. We have observed a characteristic temperature dependence for interfacial tension of the PSHQ-6,12/PDMS polymer pair, shown in Figure 8, while also directly observing homeotropic anchoring of the LCP director below and slightly above bulk isotropization. Previous theoretical work has shown that the additional free energy contribution associated with such anchoring may increase T_{NI} above the bulk value and even alter the nature of the nematic−isotropic transition to become continuous or second order.[39,40] Furthermore, if the observed homeotropic anchoring were to feature local smectic order (our observations cannot resolve this), the influence on T_{NI} would be even stronger. Indeed, Kočevar and Muševič[41] experimentally observed that a smectic-like 5CB layer near a silanated glass surface was stable even 20 °C above the clearing temperature.

Should we always expect homeotropic anchoring at a nematic−isotropic interface? From theory and simulations the answer is a matter of some debate. Doi and Kuzzu[37] and Drovetsky et al.[38] separately predict director orientation parallel to the interface, while molecular dynamics (MD) simulations[35] indicated homeotropic anchoring. Li and Denn's Monte Carlo simulations employing a three-dimensional bond fluctuation model (BFM)[32] revealed that a homeotropic arrangement featured an interfacial tension one-third that of the planar arrangement and that the former featured a more diffuse interface, discussed further below. Finally, Rey's[36] Landau−de Gennes continuum theory predicts homeotropic, planar, or oblique orientation at the interface, depending on two temperature-dependent parameters describing the anchoring energy.

Our direct observations of homeotropic nematic anchoring, shown in Figure 11, support the MD and BFM

simulation findings. Regarding the latter, Li and Denn found that the composition profile across the interface was much sharper for planar vs homeotropic far-field orientations. Surprisingly, it was further found that the order dependence (thus temperature dependence) of interfacial width was opposite for the two cases: width increasing with order for the homeotropic case but decreasing with order for the planar case (Figure 5 of ref 32). This distinct temperature dependence translated directly to the dependences of interfacial tension on order: increasing/decreasing σ with temperature/order for the homeotropic case and decreasing/increasing σ with order/temperature for the planar case. Thus, homeotropic anchoring is favored, by virtue of a lower interfacial tension, and promotes a positive $d\sigma/dT$, both features consistent with our observations.

A major question remains unanswered at this stage, however: Why do the very similar interfacial orientation states shown in Figures 10 and 11 yield, quantitatively, such different interfacial tensions as reported in Figure 8? Continued progress on the theoretical modeling of droplet dynamics, particularly for a textured LCP in an isotropic matrix with homeotropic anchoring and variable near-surface ordering, is needed and expected to improve our understanding of this interesting and technologically important problem.

Conclusion

We have determined the interfacial tension between the thermotropic nematic polymer, PSHQ-6,12, and an isotropic PDMS matrix as a function of temperature by employing modified deformed drop retraction method. Droplet retraction within the nematic phase featured a double-exponential response: a fast relaxation followed by a slower relaxation. Within the nematic phase, the interfacial tension increases slowly with temperature but then yields to a discontinuity and stepwise increase upon crossing the nematic−isotropic transition. The value of interfacial tension reaches a maximum on completion of isotropization. Within the isotropic phase, the interfacial tension decreases with temperature, following a slope of −0.3 mN/(m K). Having confirmed that PSHQ-6,12 is a negatively birefringent material, direct observation of retardance and slow-axis orientation of relaxed droplets clearly demonstrated that the nematic adopts a homeotropic orientation at the PSHQ-6,12/PDMS interface, consistent with predictions from molecular dynamic simulations,[35] a three-dimensional bond fluctuation model,[32] and a Landau−De Gennes continuum model.[36] Interestingly, we further found that nematic ordering of PSHQ-6,12 at the droplet interface was observed for temperatures well above the bulk nematic−isotropic transition. We believe that such enhancement of the nematic−isotropic transition at the interface is due to strongly anisotropic interfacial tension for PSHQ-6,12 that favors homeotropic orientation only possible so long as the nematic phase persists.

Acknowledgment. The authors gratefully acknowledge the PSHQ6,12 sample supplied by Prof. C. D. Han of University of Akron and helpful discussions with Dr. Angel Romo-Uribe of Rohm & Haas Research Laboratories. This work was supported by the National Science Foundation under Grant CTS-00093880.

Supporting Information Available: Time evolution of apparent volume for selected PSHQ-6,12 droplets in PDMS, WAXS pattern for a stretched fiber of PSHQ-6,12, and LC-Polscope retardance and orientation images for PSHQ-6,12 in PDMS. This material is available free of charge via the Internet at http://pubs.acs.org.

References and Notes

(1) Dutta, D.; Fruitwalai, H.; Kohlii, A.; Weiss, R. A. *Polym. Eng. Sci.* **1990**, *30*, 1005−1018.
(2) Weiss, R. A.; Huh, W.; Nicolais, L. *Polym. Eng. Sci.* **1987**, *27*, 684−691.
(3) Hadlos, A. A.; Baird, D. G. *J. Macromol. Sci., Part C: Polym. Rev.* **1995**, *C35*, 183−238.
(4) Tucker, C. L., III; Moldenaers, P. *Annu. Rev. Fluid Mech.* **2002**, *34*, 177−210.
(5) Krishnaswamy, S.; Shashidhar, R. *Mol. Cryst. Liq. Cryst.* **1976**, *35*, 253−259.
(6) Chen, G. H.; Springer, J. *Macromol. Rapid Commun.* **1998**, *19*, 625−629.
(7) Krishnaswamy, S.; Shashidhar, R. *Mol. Cryst. Liq. Cryst.* **1977**, *38*, 353−356.
(8) Song, B.; Springer, J. *Mol. Cryst. Liq. Cryst. Sci. Technol., Sect. A: Mol. Cryst. Liq. Cryst.* **1997**, *307*, 69−88.
(9) Rai, P. K.; Denn, M. M.; Maldarelli, C. *Langmuir* **2003**, *19*, 7370−7373.
(10) Kim, J. W.; Kim, H.; Lee, M.; Magda, J. J. *Langmuir* **2004**, *20*, 8110−8113.
(11) Chen, W. L.; Sato, T.; Teramoto, A. *Macromolecules* **1998**, *31*, 6506−6510.
(12) Boersma, A.; Van Turnhout, J. *J. Polym. Sci., Part B: Polym. Phys.* **1998**, *36*, 815−825.
(13) Machiels, A. G. C.; Busser, R. J.; Van Dam, J.; Posthuma De Boer, A. *Polym. Eng. Sci.* **1998**, *38*, 1536−1548.
(14) Xing, P. X.; Bousmina, M.; Rodrigue, D.; Kamal, M. R. *Macromolecules* **2000**, *33*, 8020−8034.
(15) Palierne, J. F. *Rheol. Acta* **1990**, *29*, 204−214.
(16) Bousmina, M. *Rheol. Acta* **1999**, *38*, 73−83.
(17) Gramespacher, H.; Meissner, J. *J. Rheol.* **1992**, *36*, 1127−1141.
(18) Lacroix, C.; Bousmina, M.; Carreau, P. J.; Favis, B. D.; Michel, A. *Polymer* **1996**, *37*, 2939−2947.
(19) Lacroix, C.; Aressy, M.; Carreau, P. J. *Rheol. Acta* **1997**, *36*, 416−428.
(20) Elemans, P. H. M.; Janssen, J. M. H.; Meijer, H. E. H. *J. Rheol.* **1990**, *34*, 1311−1325.
(21) Luciani, A.; Champagne, M. F.; Ultracki, L. A. *J. Polym. Sci., Polym. Phys. Ed.* **1997**, *35*, 1393−1403.
(22) Lee, H. S.; Denn, M. M. *Rheol. Acta* **2000**, *93*, 315−323.
(23) Mo, H. Y.; Zhou, C. X.; Yu, W. *J. Non-Newtonian Fluid Mech.* **2000**, *91*, 221−232.
(24) Son, Y. G.; Yoon, J. T. *Polymer* **2001**, *41*, 7209−7213.
(25) Taylor, G. I. *Proc. R. Soc. London, Ser. A* **1934**, *146*, 501−523.
(26) Chang, S.; Han, C. D. *Macromolecules* **1996**, *29*, 2383−2391.
(27) Chang, S.; Han, C. D. *Macromolecules* **1997**, *30*, 1656−1669.
(28) Mather, P. T.; Jeon, H. G.; Han, C. D.; Chang, S. *Macromolecules* **2000**, *33*, 7594−7608.
(29) Oldenbourg, R. *Nature (London)* **1996**, *381*, 811−812.
(30) Oldenbourg, R.; Mei, G. *J. Microsc.* **1996**, *180*, 140−147.
(31) Mather, P. T.; Pearson, D. S.; Burghardt, W. R. *J. Rheol.* **1995**, *39*, 627−648.
(32) Li, X. F.; Denn, M. M. *Macromolecules* **2002**, *35*, 6446−6454.
(33) Takeuchi, Y.; Yamamoto, F.; Shuto, Y. *Macromolecules* **1986**, *19*, 2059−2061.
(34) Larson, R. G.; Doi, M. *J. Rheol.* **1991**, *35*, 539−563.
(35) Doerr, T. P.; Taylor, P. L. *Mol. Cryst. Liq. Cryst.* **1999**, *330*, 491−501.
(36) Rey, A. D. *Phys. Rev. E* **2000**, *61*, 1540−1548.
(37) Doi, M.; Kuzzu, N. *J. Appl. Polym. Sci., Appl. Polym. Symp.* **1985**, *41*, 65−68.
(38) Drovetsky, B. Y.; Liu, A. J.; Mak, C. H. *J. Chem. Phys.* **1999**, *111*, 4334−4342.
(39) Sheng, P. *Phys. Rev. Lett.* **1976**, *37*, 1059−1062.
(40) Sheng, P. *Phys. Rev. A* **1982**, *26*, 1610−1617.
(41) Kocevar, K.; Musevic, I. *Phys. Rev. E* **2001**, *64*, 051711/1−051711/8.

MA050483X